MILITARY TECHNICAL COLLEGE
CAIRO - EGYPT

7th INTERNATIONAL CONF. ON
AEROSPACE SCIENCES &
AVIATION TECHNOLOGY

THE EFFECT OF PARTICLE SIZE ON THE STRESS AND STRAIN FIELDS IN A PLASTICALLY DEFORMED MATRIX

N. M. MAWSOUF*

ABSTRACT

Finite Element analyses of the effect of particle size on the stress and strain fields in an Al-22 wt pct Si alloy (d=100μm) are performed. The alloy was ,modified by a nucleant to obtain a more refined structure with smaller particle size (d=25μm). The general interaction between the inhomogeneity and matrix is characterized by: firstly, a hard inclusion creates a high perturbation of triaxial stress at the poles along the line of loading; secondly a hard inhomogeneity carries higher stress than the matrix; the stress level in the particle is determined by the misfit of the two phases; thirdly all the perturbation fields are scaled by inclusion size; finally a correlation has been made between the stress concentration in the matrix and the size of the in homageneity.

KEY WORDS

Metal Matrix Composites - Crack - Particles - Fracture - Stress Concentration - Strain Criterion - Nucleation

1. INTRODUCTION

Metals reinforced with particles or short fibres of hard phase exihibit a variety of failure modes during the application of monotonic or cyclic loads: (a) fracture of the reinforcing particles (b) ductile failure by the nucleation, growth, and

* Associate Professor, Dpt. of Mech. Design & Prod., Faculty of Engineering, Cairo University, Guiza, Egypt.

coalescence of voids within the metallic matrix, and (c) delamination and crack growth along the interface between the matrix and the hard phase. An understanding of the micromechanics of stress and strain inhomogeneities leading, to these failure processes is essential for improving the mechanical performance of metal-matrix- composites that are currently being used or intended for use in a number of engineering applications.

Non uniformity of deformation of two-phase material was reported by many investigators using fractographic and metallographic techniques [1-11]. Different stages of deformation, crack initiation, crackgrowth, crack propagation were examined [1-5]. The effect of particle properties: size [5-12], volume fraction [11-12], shape [12,13], and interparticle spacing [5,9], on the deformation process was studied. Some fracture mechanisms were proposed for certain materials [11-13].

In the present work, both experimental and analytical techniques were used to study the effect of particle size on the plastic deformation and fracture for the Al-22 wt% Si alloy. A relation between the stress and strain concentration around the inhomogeneity and the particle size till final fracture occurs.

2. EXPERIMENTAL AND ANALYTICAL TECHNIQUES

2.1. Material

The alloy used was prepared from a master Al-Si alloy and adding commercial purity aluminum with the proper weight and then casted and homogenized for 168 hrs at 350°C. A nucleant was added while casting, the nucleant used was phosphorous chloride with a percentage of 0.1% by weight.

2.2. Mechanical Testing

A short gauge length tensile test specimen was used. The length was 2 mm and 4 mm in diameter. Both optical and SEM microscopes were used to study the fracture surface and the area under fracture by taking longitudinal sections.

2.3. Finite Element Model

A finite element model was constructed having the same volume fraction but different particle sizes. The number of nodes=120, and the number of elements=198 as shown from Fig.1 . The boundary conditions for the finite

element model is shown in Fig.1 . The finite element plate model was subjected to nonlinear elastic plastic deformations.
A plane stress two dimensional plate model was used. The plate model is a rectangle of sides=0.220, 0.180 mm, and area of 0.0396 mm^2. The volume fraction of sillicon content is 25% and the volume percentage of sillicon particles=12.5%. For the larger particle size alloy: particle size = 100 μm and the number of particles in the model = 1 particle. For the smaller particle size alloy, particle size = 25 μm and the number of particles in the model = 16 particles. The physical properties used in the computer program were obtained from the metals handbook [18] as follows:

Table 1. Physical properties

	eutectic medium	Silicon Particles
Young's modulus "E" (GN/m^2)	72.43	108.93
Poisson's ratio "ν"	0.33	0.20
Yield strength "σy" (MN/m^2)	62.79	94.73
Ultimate tensile strength "σu" (MN/m^2)	246.13	94.73

3. RESULTS AND DISCUSSIONS

3.1. Microscopic Observations

Figure 2. shows typical microstructure for the Al-22 wt% Si alloy. It consists of the hard silicon particles embedded in a ductile eutectic matrix.

The fracture surface for the alloys was examined using the SEM as shown from Figure 3. Fracture occurred by cleavage of the silicon particles and by ductile fracture in the matrix. Intense stress and strain distributions occurred around the particles. Thicker slip lines occurred in the larger particle size alloy. Many secondary cracks were observed from Fig.3. (a,b,c,d), also some circumferential cracks on the cylindrical surface occurred trying to propagate towards the center of the specimen. The crack size is equal to the particle size Fig.3 (e,f). This explains the difference of the ultimate tensile strength for the two alloys.

3.2. Stress-Strain Curves

Stress-strain curves were obtained using both experimental and analytical techniques Fig.4. shows the unnucleated and nucleated conditions. The Ultimate tensile strength for the alloy of larger particle size is about 75% of that of smaller

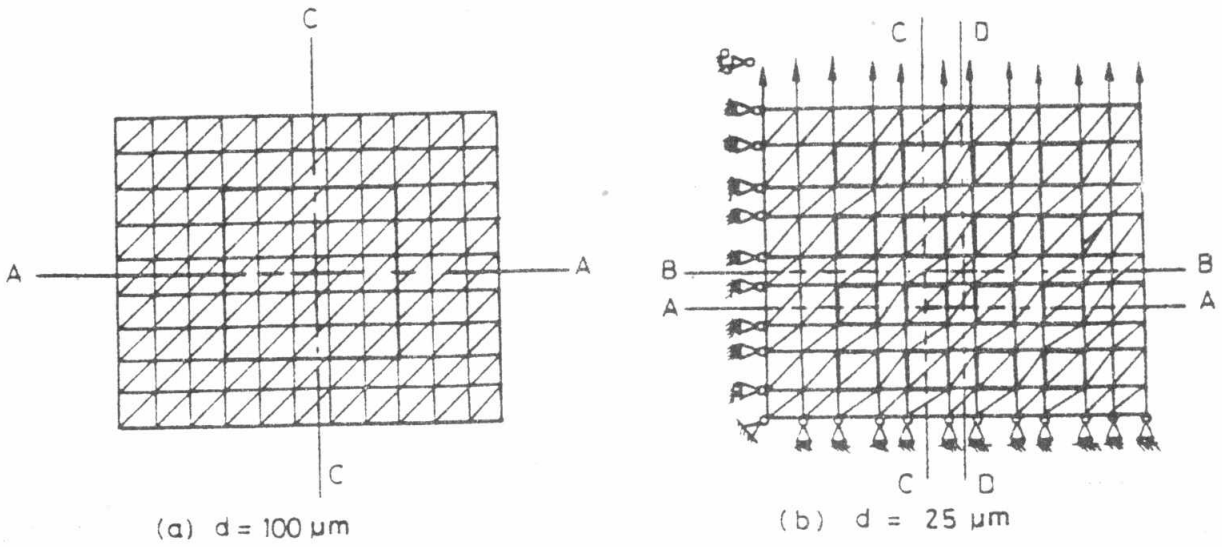

Fig.1. FEM idealization

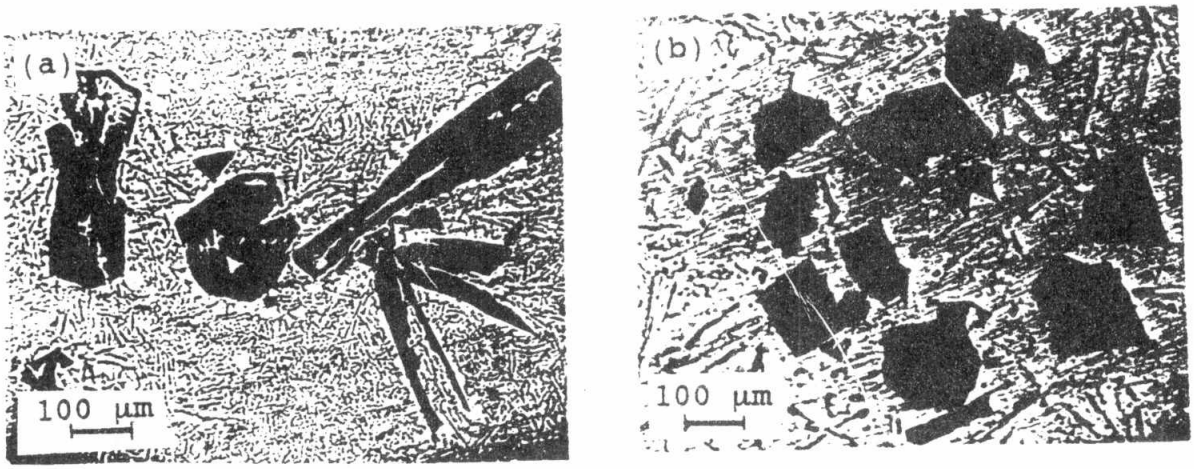

Fig.2. Microstructure of the Al-22wt% Si Alloy.
(a) Unnucleated (d=100µm) (b) Nucleated (d=25µm)

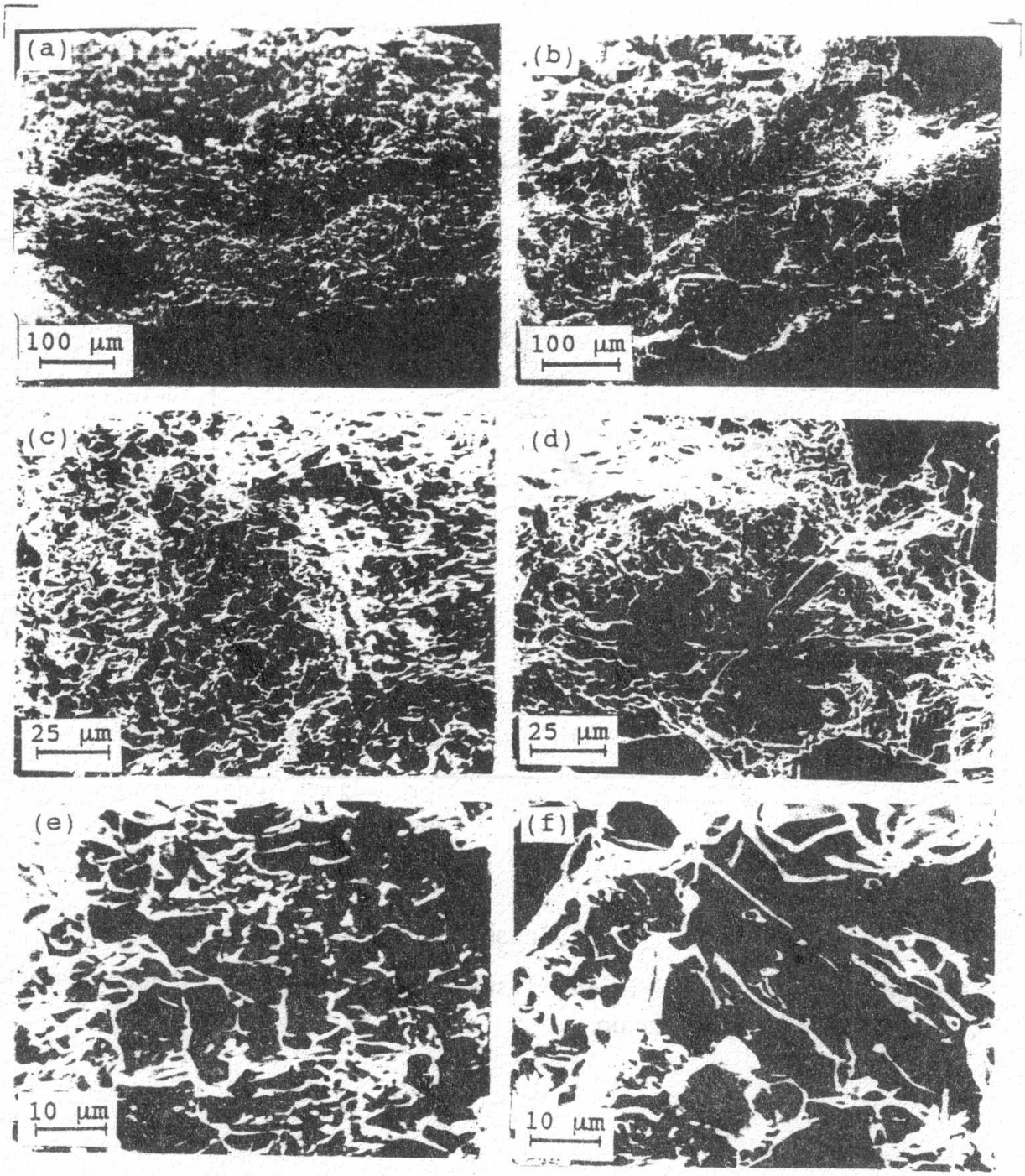

Fig.3. Fracture surface showing the cleavage cracking of silicon particles and the ductile fracture of the matrix. (a),(c),(e) particle size (d=25μm); (b),(d),(f) particle size (d=100μm).

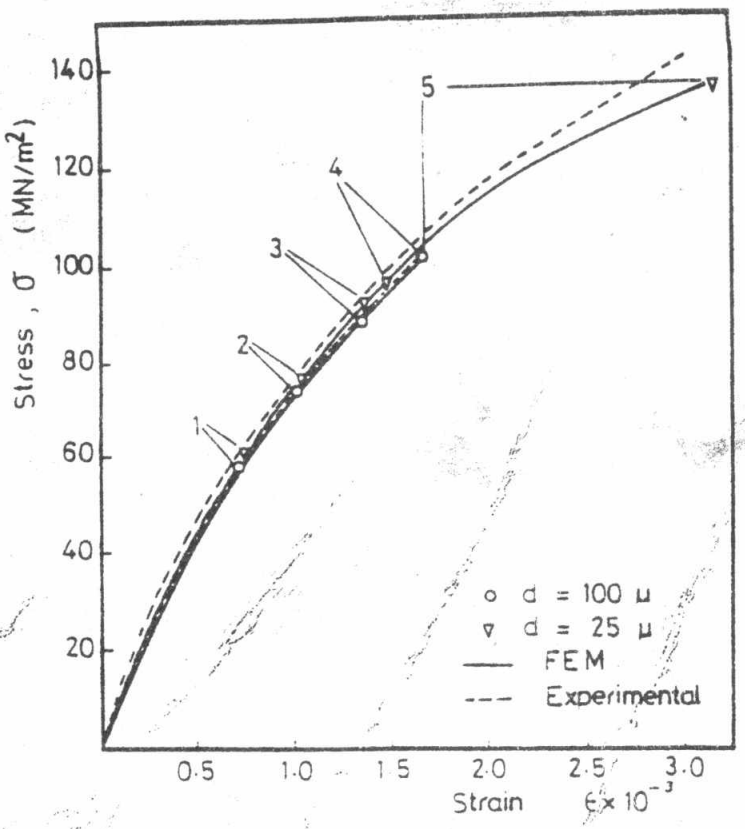

Fig.4. Stress Strain Curve

(1) Start of yield, (2) end of yield, (3) start of particle cracking, (4) end of particle cracking, and (5) Final fracture.

particle size alloy. The elongation percent for the alloy of larger particle size is about 50% of that of smaller particle size alloy.

3.3. Finite Element Method

The FEM results give the propagation of the plastic deformation in the matrix as shown from Fig.5. Plastic deformation started around the particle in the tensile direction. The matrix reaches the fully plastic deformation before any crack occurrence in either alloys. Complete plastic deformation of the matrix occurs at

lower stress and strain values for the larger particle size alloy. After both alloys suffer some plastic strain, particle cracking starts. Fracture and separation of the material occurs earlier in the case of larger particle size alloy. The lower particle size alloy undergoes some plastic deformation of the matrix after complete cracking of its particles, then separation or final fracture of the material occurs as shown from Fig. (5,6,7,8).

Figure 9 gives the relation between the percentage matrix area which is deformed plastically "$A_{m.pl}$" to the total area of the matrix "A_{mtot}" versus stress and strain. The two alloys have almost the same behavior in this stage.

Figure 10 shows the cracking stage of silicon particles. For the large particle size alloy cracking occurs first at lower stress and strain than the other alloy. The crack grew very fast at a higher rate and final fracture of the material occurred at about 60% of cracked silicon elements. The cracking of the smaller particle size alloy gives a straight line relation and crack grew at lower constant rate. The material continues deforming after all the silicon particles were cracked till final separation occurs at higher stress and strain than the larger particles size alloy.

This can be explained by: cracking of material containing hard particles embedded in a ductile matrix undergoes three stages: (1) Crack initiation at larger hard particles, (2) Crack growth from the large crack particles trying to overcome the matrix blunting and also the occurrence of cracks at smaller particles at lower rate than the previous stage, (3) Coalescence of large cracks leading to final fracture [1].

For the large particle size alloy, once crack is initiated, it grows very fast, because of its large crack size, leading to final fracture, This means that the alloy undergoes stage II of high crack growth rate while the smaller particle size alloy is still at stage I cracking of the lower rate at the same stress and stain condition Fig. 10.

For the lower particle size alloy, it was assumed for the FEM that the particles are equally spaced and of equal size. So the material undergoes the crack initiation, growth and coalescence with the same rate. Then the material suffers more deformation till final fracture occurs. The fracture stress and strain for both alloys were found to have the relations:

$$\sigma_u\,(d=100\mu m) = 75\%\ \sigma_u\,(d=25\ \mu m)\ \&\ \varepsilon_u\,(d=100\mu m) = 50\%\ \varepsilon_u\,(d=25\mu m) \quad (1)$$

These values are explained by the values of crack size given in the form of particle size. $d_{larger} = 4\ d_{smaller}$. From the fracture mechanics it can be seen that the critical

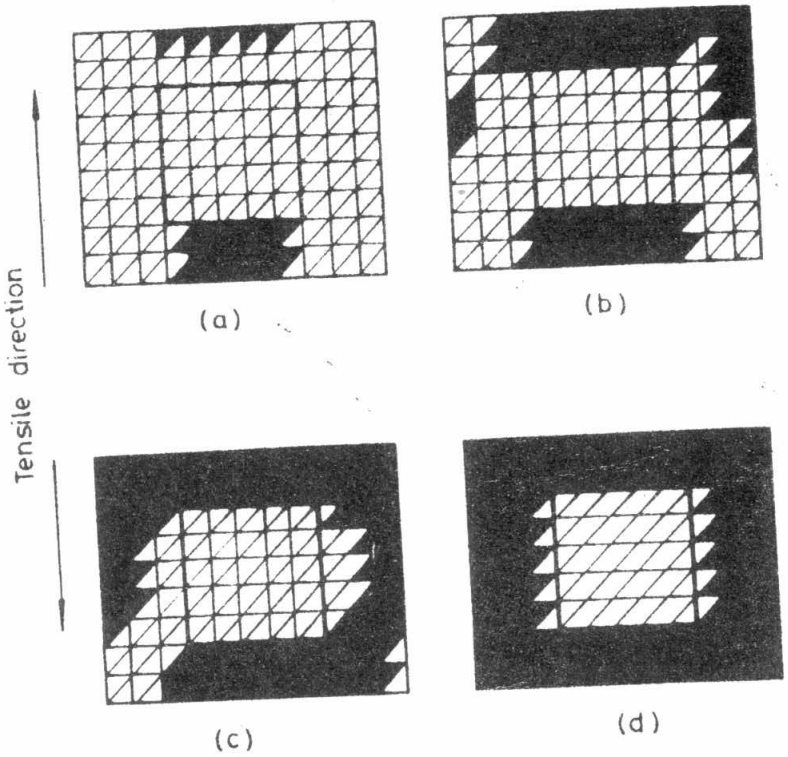

Fig.5. Progress of the plastic deformation of the matrix for the un-nucleated alloy (d=100μm)

(a) y% = 13.5%, $\varepsilon=0.74\times10^{-3}$, $\sigma=59.2$ MN/m^2
(b) y% = 48.7%, $\varepsilon=0.81\times10^{-3}$, $\sigma=63.4$ MN/m^2
(c) y% = 74.3%, $\varepsilon=0.85\times10^{-3}$, $\sigma=65.5$ MN/m^2
(d) y% = 93.2%, $\varepsilon=0.94\times10^{-3}$, $\sigma=70.3$ MN/m^2

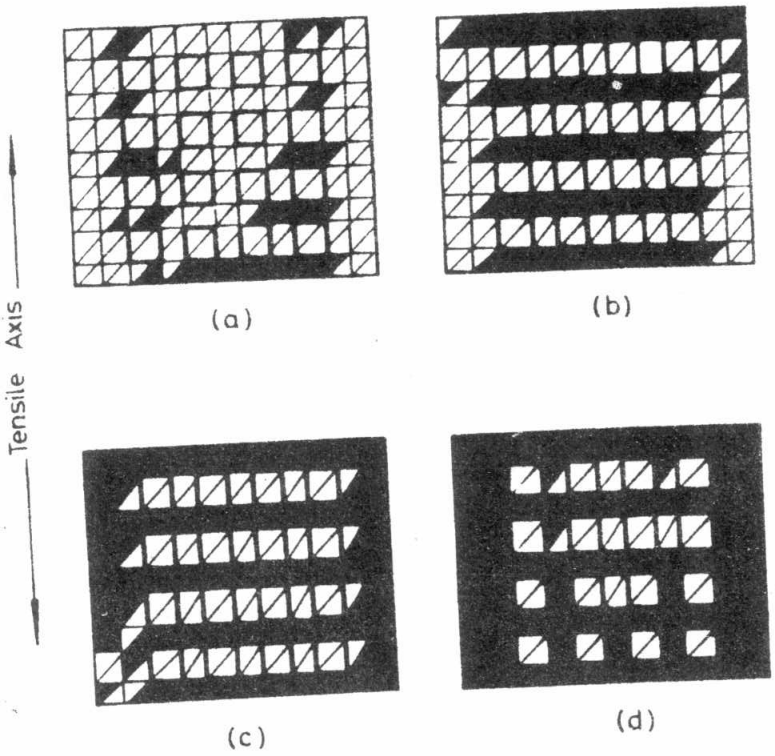

Fig. 6. Progress of the plastic deformation of the matrix for the nucleated alloy (d=25μm)

(a) y% = 20.9%, $\varepsilon=0.76\times10^{-3}$, $\sigma=61.0$ MN/m^2
(b) y% = 49.0%, $\varepsilon=0.801\times10^{-3}$, $\sigma=63.8$ MN/m^2
(c) y% = 75.7%, $\varepsilon=0.85\times10^{-3}$, $\sigma=66.8$ MN/m^2
(d) y% = 93.0%, $\varepsilon=1.01\times10^{-3}$, $\sigma=74.9$ MN/m^2

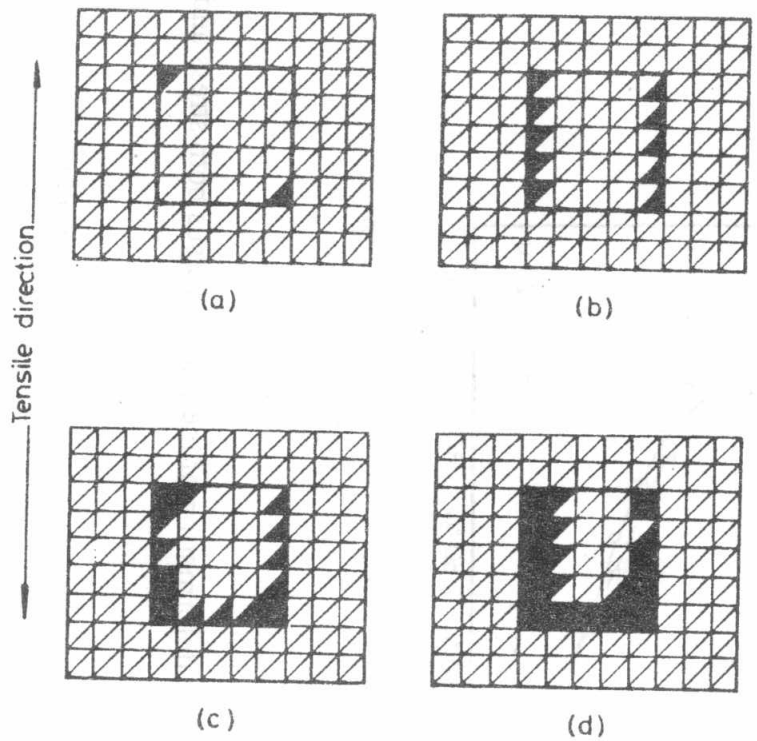

Fig.7. Cleavage cracking of silicon particles for the unnucleated alloy. (d=100μm)

(a) c% = 4%, ε=1.37x10^{-3}, σ= 89.51 MN/m^2, n% = 100%
(b) c% = 20%, ε=1.48x10^{-3}, σ= 95.01 MN/m^2, n% = 100%
(c) c% = 36%, ε=1.60x10^{-3}, σ= 100.26 MN/m^2, n% = 100%
(d) c% = 60%, ε=1.66x10^{-3}, σ= 102.58 MN/m^2, n% = 100%

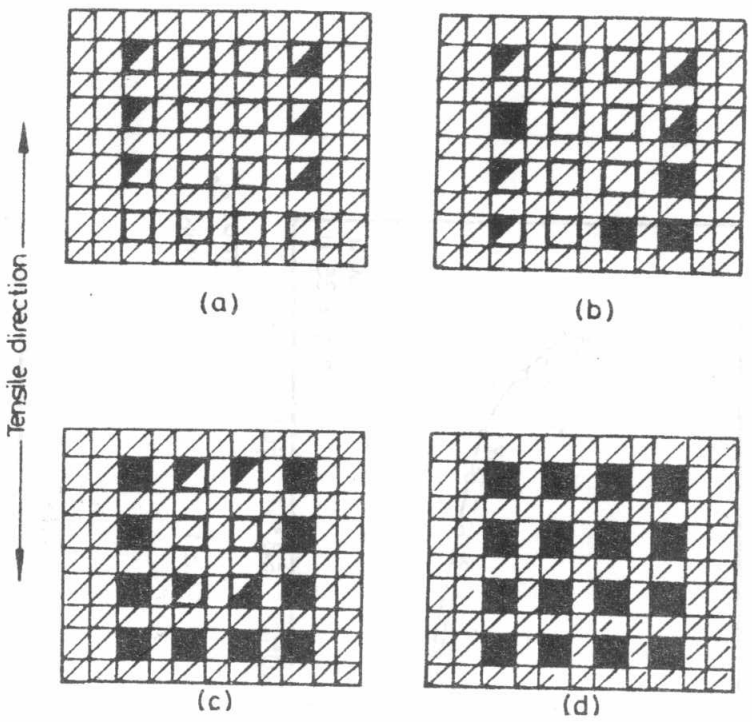

Fig.8. Cleavage Cracking of silicon particles for the nucleated alloy. (d=25μm)

(a) c% = 18.75% , ε=1.38x10^{-3}, σ= 92.62 MN/m^2, n% = 37.50%
(b) c% = 40.63% , ε=1.41x10^{-3}, σ= 94.22 MN/m^2, n% = 56.25%
(c) c% = 75.00% , ε=1.44x10^{-3}, σ= 95.42 MN/m^2, n% = 87.50%
(d) c% = 100.00% , ε=1.48x10^{-3}, σ= 96.58 MN/m^2, n% = 100.00%

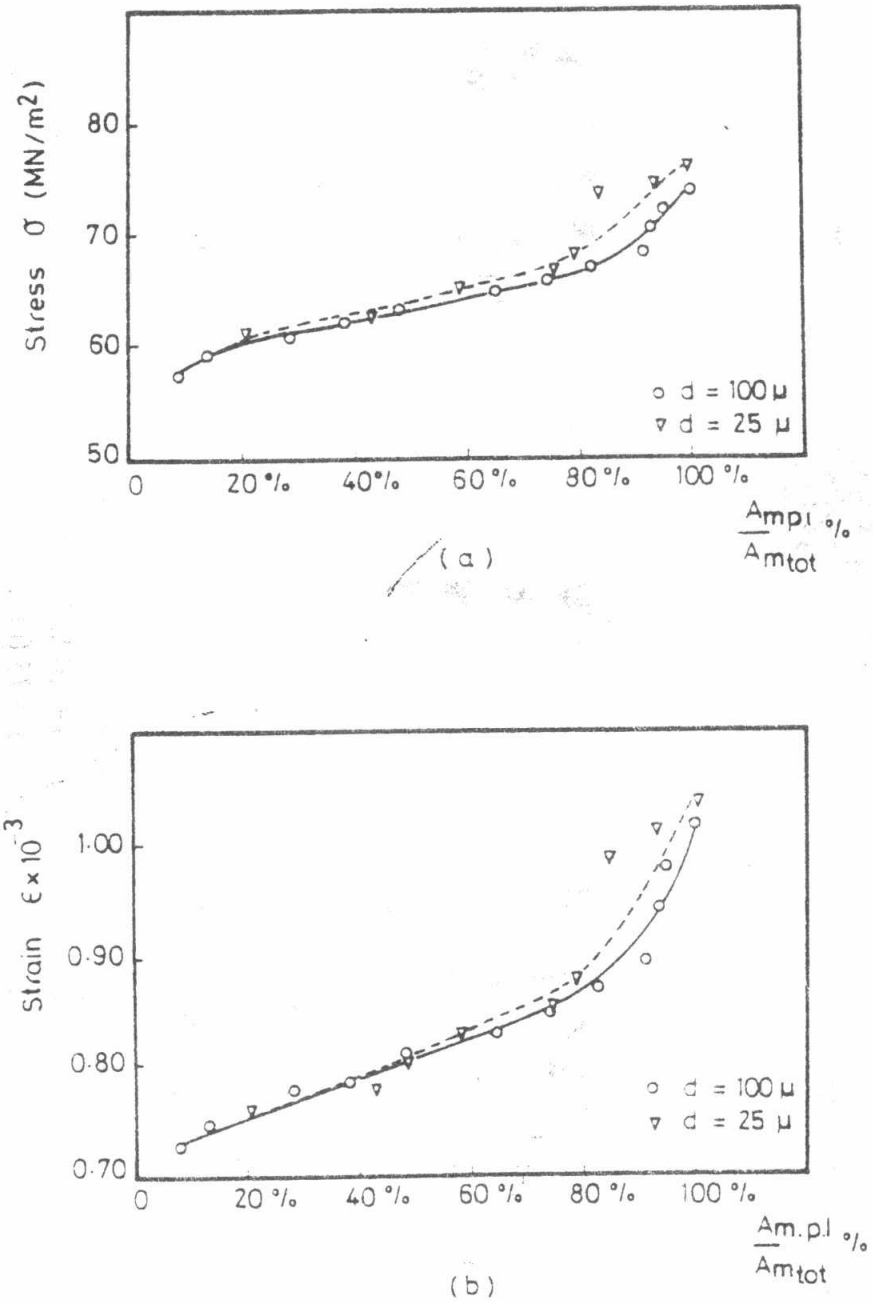

Fig.9. The propagation of plastic deformation of the matrix versus both stress and strain.

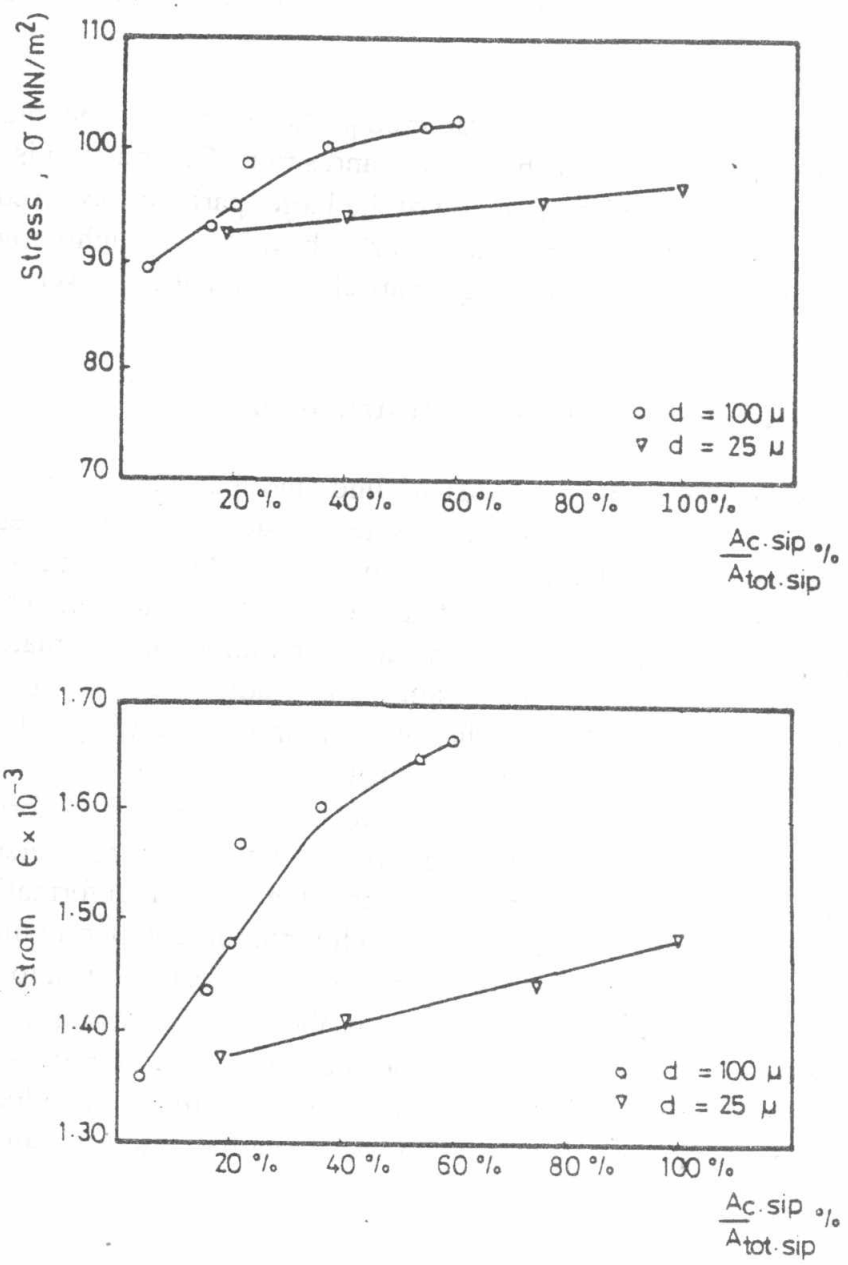

Fig.10. Propagation of crack of silicon particles versus both stress and strain.
A_c Sip = area of elements of cracked silicen particles
A_{tot} Sip= total area of elements of silicon particles.

stress to cause fracture is inversely proportional to the square root of the crack size, the critical stress intensity factor K_{IC} the interparticle spacing, the orientation of particles, etc. [6,7]. This can give an idea about the difference in the ultimate stress values.

Figure 11 showed the number of the fractured particles "$N_{f.p}$" to the total number of particles "$N_{tot.p}$" percent versus both stress and strain. This relation is linear for the d=25μm alloy and complete cracking of the larger particles occurred at lower stress and strain. Also the experimental work showed severe inhomogeneity of stress and strain distributions around larger particles than that for lower ones.

3.4. Inhomogeneity of Stress and Strain Distributions

Stress and strain inhomogenuous fields around hard particles were examined in terms of different stages of deformation. These stages were (a) the beginning of plastic deformation in the ductile matrix, (b) the eutectic medium is completely plastic, (c) the beginning of cracking of hard particles, (d) the complete cracking of hard particles or the final fracture and separation of the material. This inhomogeneity of both stresses and strains was studied in two directions, the tensile direction and the transverse direction as shown from Figs. (12-17). This inhomogeneity was more severe in the tensile direction Fig.13 than that in the transverse direction Fig.12(a). The strain ratio showed value of ≈2 for the tensile direction Fig.13, while the strain ratio was about ≈ 1.5 for the transverse direction Fig.12. These values increase by increasing the overall deformation of the material. The stress ratio did not show much variation comparing the value for both directions. In the transverse direction, the stress ratio showed to be ≈ 1.1 in average, while in the tensile direction it was about ≈ 1.2 in average. Also at the interface between silicon particles and the eutectic medium the stress and strain values were higher than its values at the inside for the silicon particle. The stress and strain values at the interface were lower than the interior values for the eutectic medium Fig.12.

To study stress and strain inhomogeneity in the case of smaller particle size alloy four sections (A,B,C,D) were studied as shown from Fig.15 stress and strain inhomogeneity were studied at the four stages of deformation mentioned before. Figs.(14,15) show the stress and strain distributions for sections (A-A,C-C) respectively. Figs (16,17) show the stress and strain distributions for sections (B,D) respectively. The stresses showed higher values in the eutectic medium compared to that of the silicon particles. The ratio between the maximum value to the minimum value was about ≈ 1.2 in the tensile direction Figs. (15,17) while this stress ratio value was about ≈ 1.1 in the transverse direction Figs. (14,16). The strain inhomogeneity was more severe than the stress inhomogeneity. The silicon

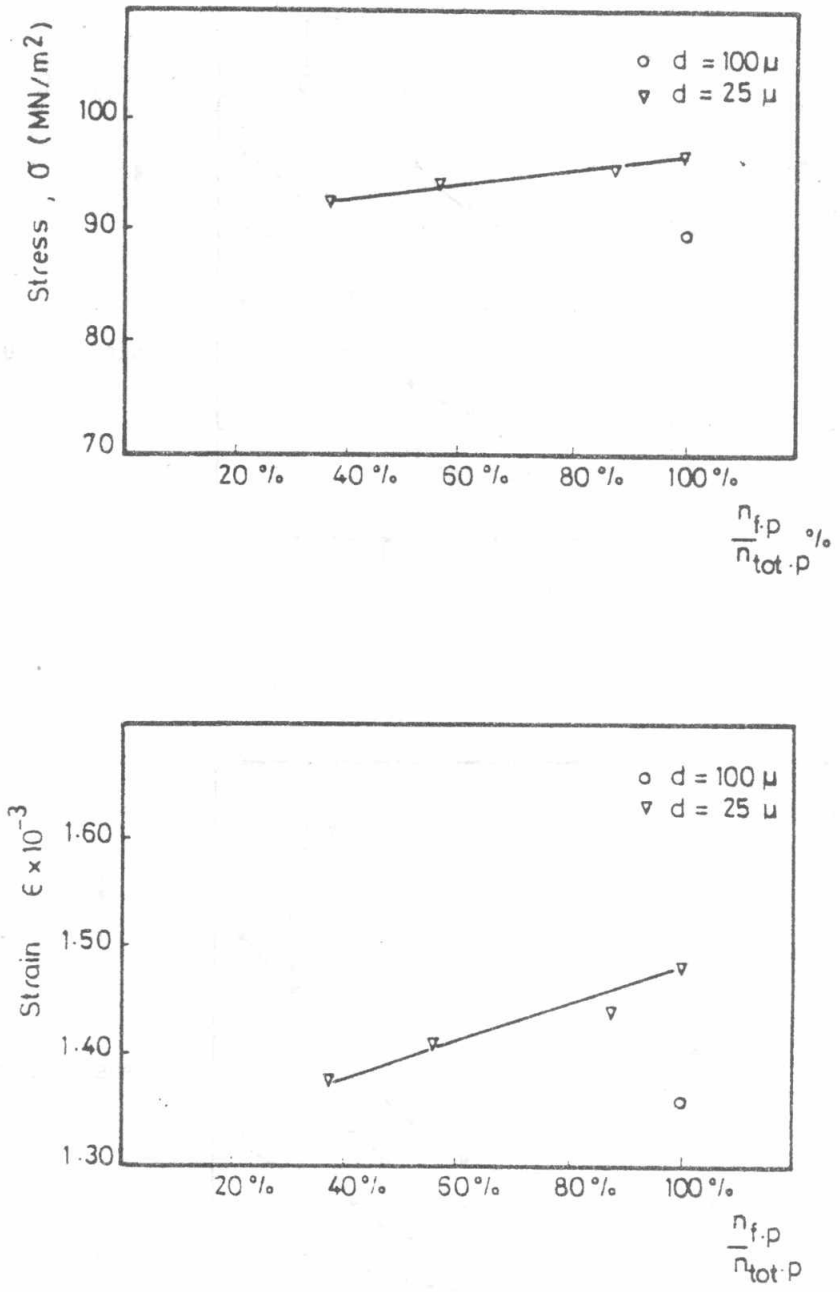

Fig.11. Number of fractured particles percent versus both stress and strain.

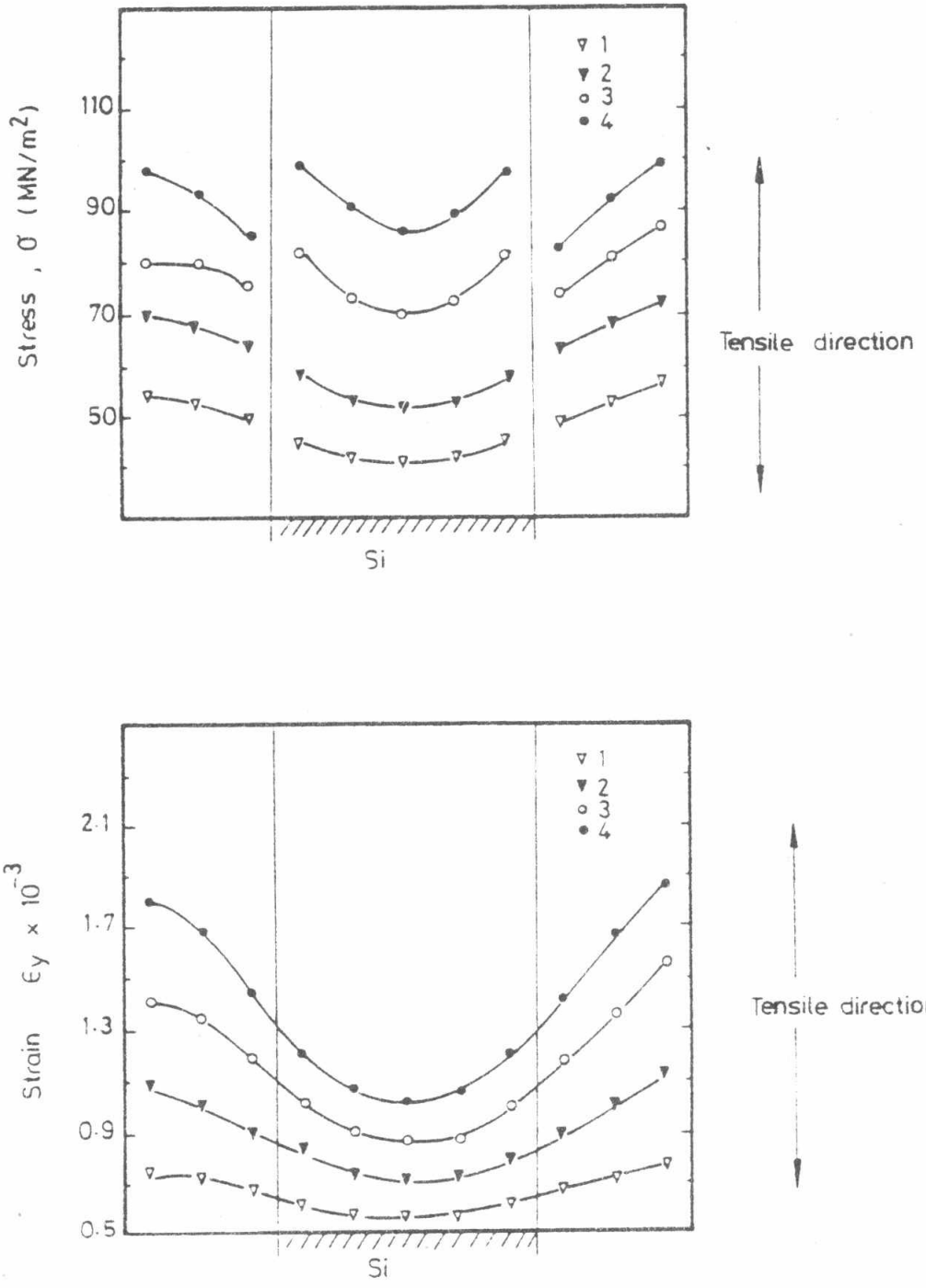

Fig.12. Stress and strain distributions along sec. (A-A) for the larger particle size alloy (d=100μm). 1,2,3,4 indicate the beginning of matrix plastic deformation, total matrix plastic deformation, start of particle cracking, and end of particle cracking as given from figure 4.

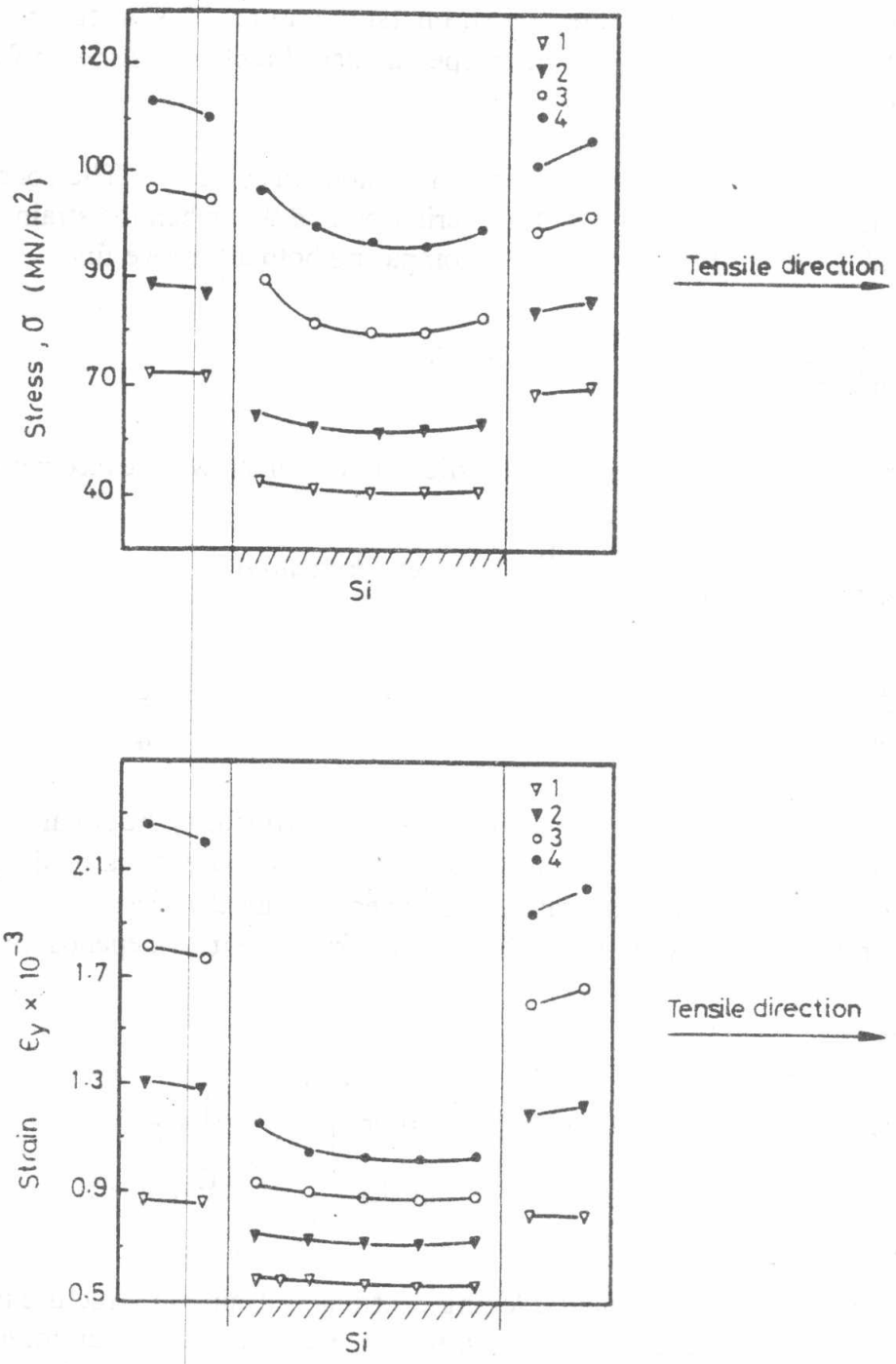

Fig.13. Stress and strain distributions along sec. (C-C) for the larger particle size alloy (d=100μm). 1,2,3,4 indicate the beginning of matrix plastic deformation, total matrix plastic deformation, start of particle cracking, and end of particle cracking as given from figure 4.

particles suffered lower strain than the eutectic medium. The ratio between the maximum and minimum values of strain (strain ratio) was about ≈ 1.5 in the tensile direction and ≈ 1.1 in the perpendicular direction as shown from Figs. (14,15,16,17).

From the previous discussion a final conclusion was obtained. The conclusion is that the fracture criterion is a strain criterion and that when the strain reaches a critical value the final fracture occurs. Comparing both alloys we find.

$$\frac{\text{The strain ratio } (d = 25\mu m)}{\text{The strain ratio } (d = 100\mu m)} = \frac{1.5}{2} = 0.75 \qquad (2)$$

in the direction perpendicular to the tensile axis which showed severe perturbation

$$\frac{\text{The fracture stress } (d = 100\ \mu m)}{\text{The fracture stress } (d = 25\ \mu m)} = 0.75 \text{ (experimental)} \qquad (3)$$

$$\frac{\text{The fracture strain } (d = 100\ \mu m)}{\text{The fracture strain } (d = 25\ \mu m)} = 0.5 \text{ (experimental)} = \sqrt{\frac{d_{smaller}}{d_{larger}}} \qquad (4)$$

The ratio for the fracture strains is inversely proportional to the square root of the particle size. The fracture stress is related to the fracture strain by the parabolic relation $\sigma = a\varepsilon^b$ (from experimental results) where a,b are constants.
which agrees with experimental work. So the fracture stress depends inversely on the root square of the particle size.

$$\frac{\text{The fracture stress } (d = 100\ \mu m)}{\text{The fracture stress } (d = 25\ \mu m)} = \left(\frac{\varepsilon_{larger}}{\varepsilon_{Smaller}}\right)^b = \left(\frac{d_{smaller}}{d_{larger}}\right)^{\frac{b}{2}} = 0.75 \qquad (5)$$

Also it depends on the strain hardening coefficient. Using the fracture mechanics approach for calculating the "J" integral for the elastic plastic aluminium alloy, it was found that it depends on the particle size and the strain hardening coefficient.

The ratio of the ultimate tensile strength of both alloys was 75% which agrees inversely with the strain concentration ratio between both alloys measured in the tensile direction which was also equal to 75%. This explains the role of particle size on the tensile strength of the material and the inhomogeneity resulted from the existence of the hard particles.

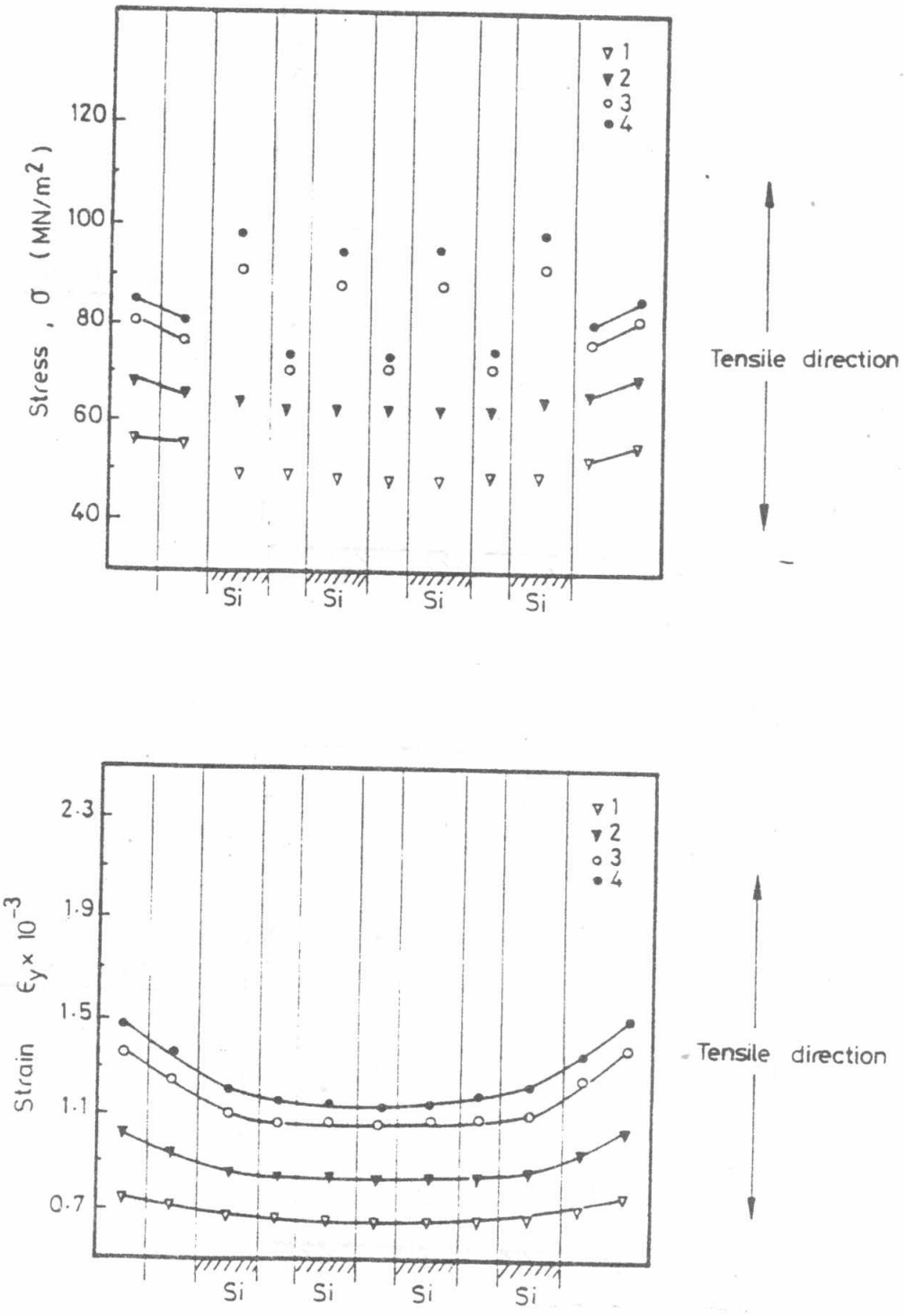

Fig.14. Stress and strain distributions along sec. (A-A) for the smaller particle size alloy (d=25μm). 1,2,3,4 indicate the beginning of matrix plastic deformation, total matrix plastic deformation, start of particle cracking, and end of particle cracking as given from figure 4.

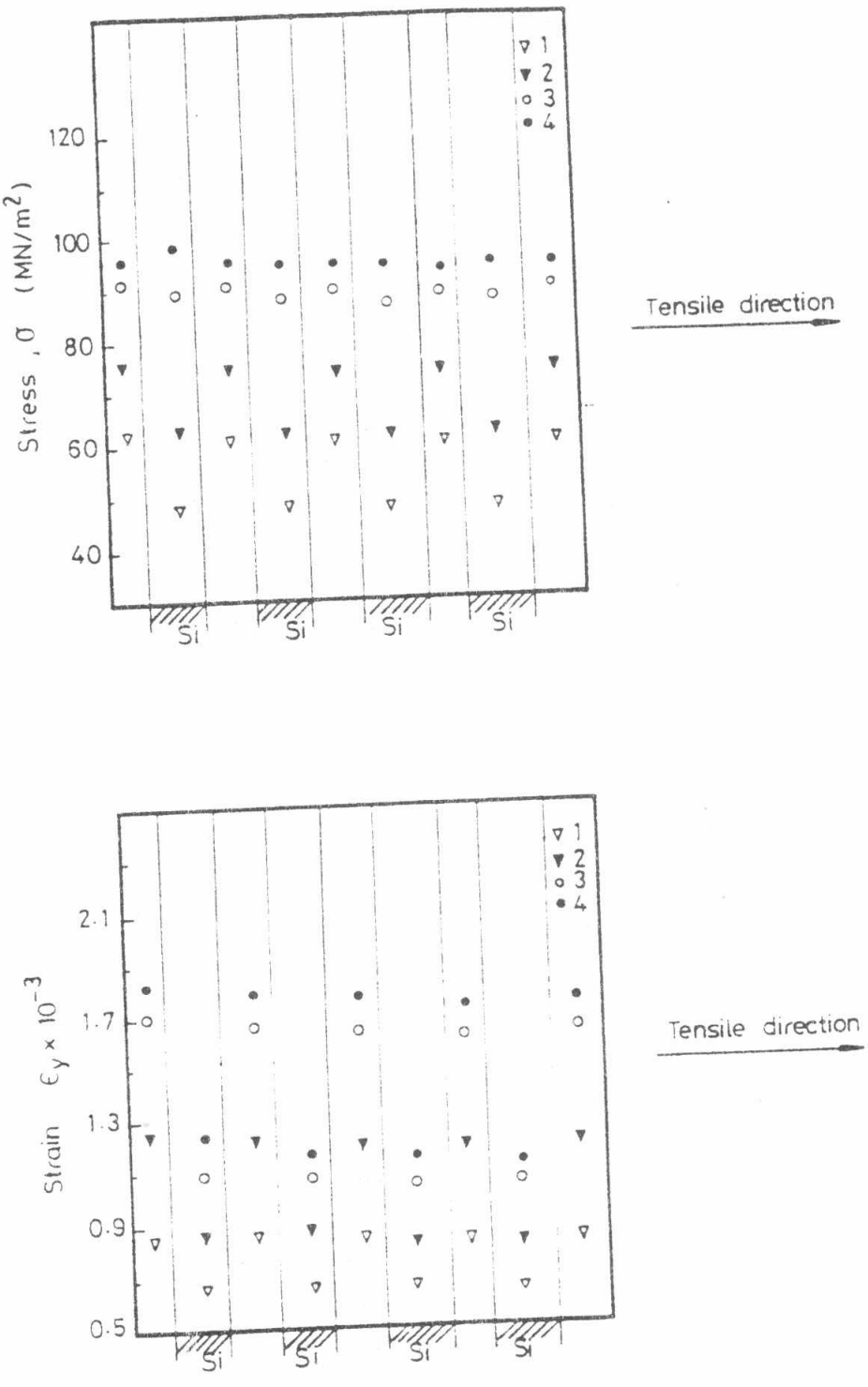

Fig.15. Stress and strain distributions along sec. (C-C) for the smaller particle size alloy (d=25μm). 1,2,3,4 indicate the beginning of matrix plastic deformation, total matrix plastic deformation, start of particle cracking, and end of particle cracking as given from figure 4.

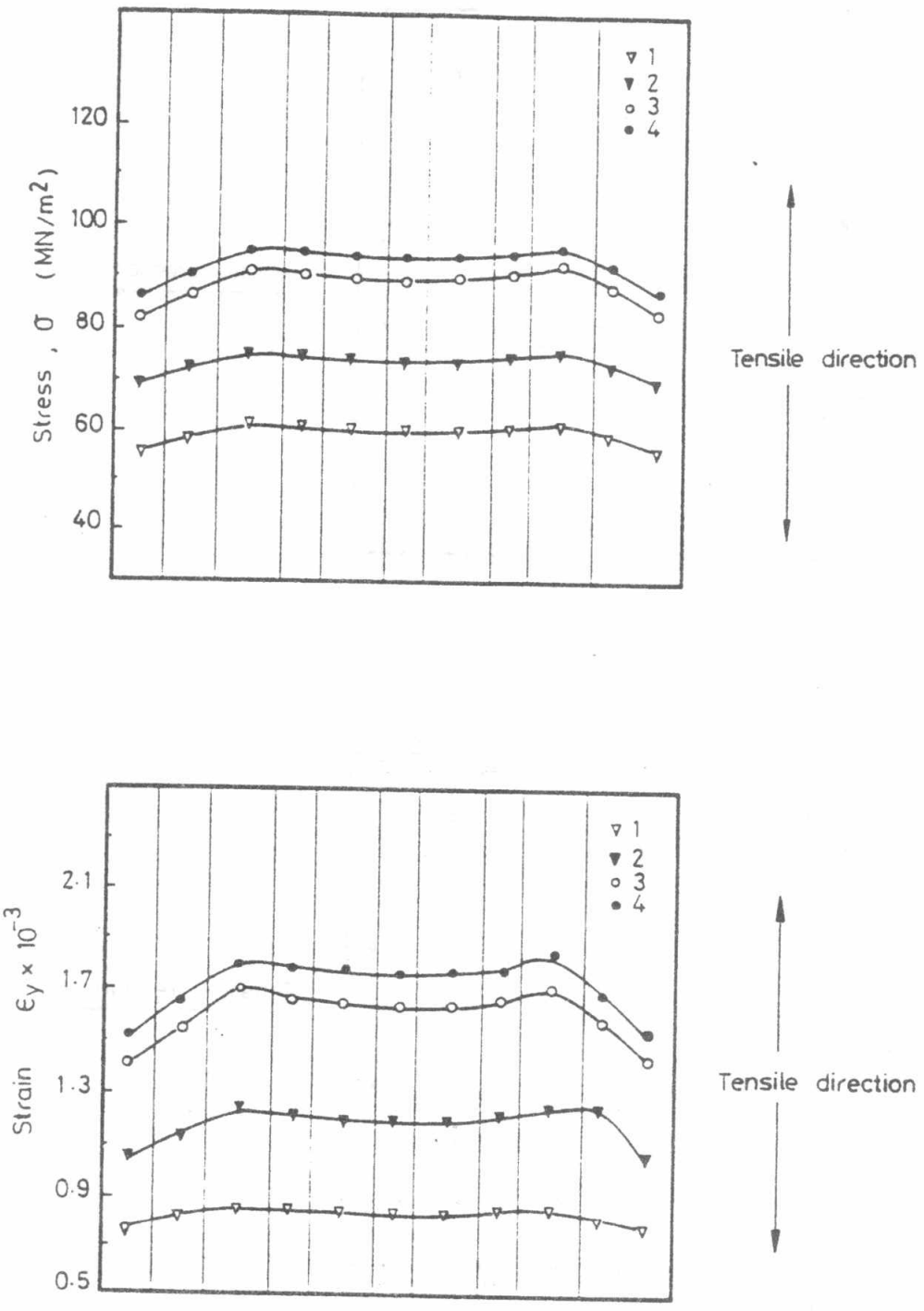

Fig.16. Stress and strain distributions in the eutectic matrix along sec. (B-B) for the smaller particle size alloy (d=25μm). 1,2,3,4 indicate the beginning of matrix plastic deformation, total matrix plastic deformation, start of particle cracking, and end of particle cracking as given from figure 4.

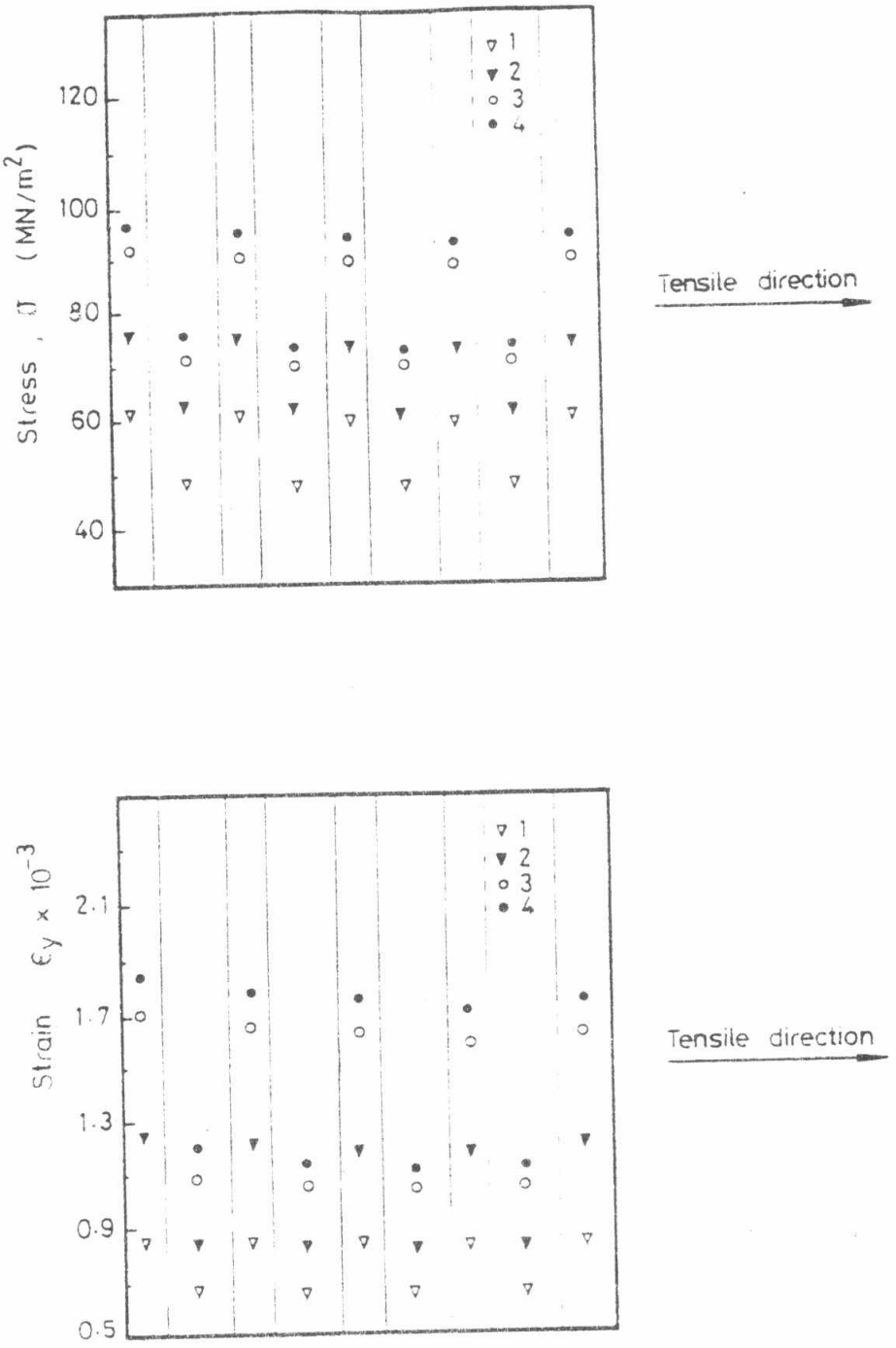

Fig.17. Stress and strain distributions in the eutectic matrix along sec. (D-D) for the smaller particle size alloy (d=25μm). 1,2,3,4 indicate the beginning of matrix plastic deformation, total matrix plastic deformation, start of particle cracking, and end of particle cracking as given from figure 4.

4. CONCLUSIONS

(1) Silicon particles carries higher tensile stress than the eutectic matrix. As expected, the silicon particle deforms less than the aluminium matrix.
(2) The highest stress value in the matrix is located at the interface along the line of loading. The highest strain magnitude is also located at the interface along the line of loading.
(3) Lobe regions of low stresses and strains are existed at the side of a particle.
(4) The maximum stress and strain perturbations were found in the direction of loading at the interface and is measured in terms of strain and stress concentration ratios.
(5) Strain ratio ≈2 for larger particle size alloy
≈1.5 for smaller particle size alloy.
(6) The ultimate tensile stress for large paticle size alloy ≈ 0.75 the ultimate tensile stress for the smaller particle size alloy.
(7) The fracture stress is inversly proportional to the square root of the particle size.
(8) Finally it has been shown that all the stress and strain perturbation fields are scaled by the particle size.

REFERENCES

[1] Mawsouf, N.M., "Study of the Tensile Fracture Mechanism and Prediction of the Fracture Criterion in Aluminum Alloys", J. of Mater. Science Letters, Vol.12, pp. 128-131 (1993).
[2] Kwon, D. and Asaro, R. J., "A Study of Void Nucleation, Growth and Coalescence in Spherodized 1518 Steel.", Metall. Trans. A, 21A pp 117-134 (1990).
[3] Doong, S.H., Lee, T.C., Robertson, I.M. and Birnbaum, H.K., "Dynamic Studies of the Crack Initiation and Growth Mechanisms in Al/Si Cp Composites", Scripta Metall., 23 pp. 1413-1418 (1989).
[4] Cox T.B. and Low, J.R., Jr., "An Investigation of the Plastic Fracture of AISI 4340 and 18 Nickle-200 Grade Maraging Steels", Metall. Trans., 5 pp.1457-1470 (1974).
[5] Watt, D.F., Xu, X.Q., and Lloyd, D.J., " Effect of Particle Morphology and Spacing on the Stress and Strain Fields in a Plastically Deforming Matrix", Acta mater., Vol.44, No.2, pp. 789-799 (1996).
[6] Xu, X.Q., and Watt, D.F., "Basic Role of a Hard Particle in a Metal Matrix Subjected to Tensile Loading", Acta, metall., mater., Vol.42, No.11, pp. 3717-3729 (1994).

[7] Finot. M.. Shen. Y.L.. Needleman. A.. and Suresh. S.. Metall and Mater. Trans.. Vol.25A. (1994) 2403.
[8] Caceres. C.H.. and Grittiths. J.R.. Acta mater.. Vol.44. No.1 (1996).
[9] Kamat. S.V.. Hirth. J.P.. and Mehrabian. R.. Acta Metall.. 37 (1989) 2395.
[10] Vijayaraghavan. T.V.. and Margolin. H.. Metall. Trans. A. 19A (1988) 1311.
[11] You. C.P.. Thompson. A.W.. and Bernstein. I.M.. Scripta Metall.. 21 (1987) 181.
[12] Margolin . H.. and Vijayaraghavan. T.V.. Metall. Trans. A. 14A (1983) 2043.
[13] Rittel. D.. and Roman. I.. Metall. Trans. A. 19A (1988) 2269.
[14] Butcher. B.R.. and Allen. P.L. Metal Science (1977) 462.
[15] Ankem. S.. and Margolin. H.. Metall. Trans. A. 13A (1982) 603.
[16] Ankem. S.. and Margolin. H.. J. of Metals. 38 (1986) 25.
[17] Lin. T., Evans. A.G., and Ritchie. R.O., Metall. Trans. A. 18A (1987) 641.
[18] Metals Handbook 1984.